

Isogeometric Collocation Method for the Fractional Laplacian in the 2D Bounded Domain

Kailai Xu^a, Eric Darve^{a,b}

^a*Institute for Computational and Mathematical Engineering, Stanford University, Stanford, CA, 94305*

^b*Mechanical Engineering, Stanford University, Stanford, CA, 94305*

Abstract

We consider the isogeometric analysis for fractional PDEs involving the fractional Laplacian in two dimensions. An isogeometric collocation method is developed to discretize the fractional Laplacian and applied to the fractional Poisson problem and the time-dependent fractional porous media equation. Numerical studies exhibit monotonous convergence with a rate of $\mathcal{O}(N^{-1})$, where N is the degrees of freedom. A comparison with finite element analysis shows that the method enjoys higher accuracy per degree of freedom and has better convergence rate. We demonstrate that isogeometric analysis offers a novel and promising computational tool for nonlocal problems.

Keywords: Isogeometric Analysis, Fractional Laplacian, Singularity Subtraction

1. Introduction

We consider the two-dimensional nonlocal model involving the Riesz fractional Laplacian, which can be defined through the Fourier transform [28]

$$\mathcal{F}((-\Delta)^s u)(\boldsymbol{\xi}) = |\boldsymbol{\xi}|^{2s} \mathcal{F}(u)(\boldsymbol{\xi}) \quad (1)$$

where $s \in (0, 1)$, \mathcal{F} is the Fourier transform, and u is sufficiently smooth. Equivalently, we have

$$(-\Delta)^s u(\mathbf{x}) = c_{s,2} \text{p.v.} \int_{\mathbb{R}^2} \frac{u(\mathbf{x}) - u(\mathbf{y})}{|\mathbf{x} - \mathbf{y}|^{2+2s}} d\mathbf{y} \quad (2)$$

where p.v. denotes principal integration and $c_{s,2}$ is the normalization constant

$$c_{s,2} = \frac{2^{2s} \Gamma(1+s)}{\pi |\Gamma(-s)|} \quad (3)$$

The nonlocal models naturally arise from many physical processes that exhibit super-diffusive jump phenomena. However, the computational methods for nonlocal models lag drastically

Email addresses: kailaix@stanford.edu (Kailai Xu), darve@stanford.edu (Eric Darve)

behind their integer-order counterparts and are generally more expensive in both storage and computational cost. Thus, the integer-order differential equations are usually used as approximations in physical modeling. Recently with more computational resources available, interests are shifting back to nonlocal models. Many applications can be modeled by partial differential equations involving the fractional Laplacian, such as the reverse time migration (RTM) for attenuating media [40], the anomalous diffusion in porous media [12], and image denoising [15]. For a more comprehensive treatment involving the theory and numerical methods of fractional Laplacian, we refer readers to the review paper [30].

It is worth mentioning that many other formulations of fractional operators for nonlocal models exist [21, 20]. For example, the time-fractional models [22, 24] and the space-time fractional models [23] are two alternative fractional operators to the fractional Laplacian operator. The differential operators in the aforementioned fractional operators are usually decoupled in time or space. In contrast, the two spatial dimensions of the fractional Laplacian operator Eq. (2) cannot be decoupled and must be considered altogether in the numerical discretization, which poses unique challenges.

The challenges in solving the fractional partial differential equations involving the fractional Laplacian is many folds. Firstly, the kernel Eq. (2) is singular and therefore requires techniques like computing singular integrals in the boundary element method. The corresponding implementation can be quite challenging, especially in the case where the computational domain is complex and high dimensional. For example, Acosta et al. [2] developed a nontrivial finite element method by applying the Duffy-type transforms and different quadrature rules according to the relative position of two triangle elements (i.e., identical, sharing a vertex, sharing an edge and disjoint). Secondly, with homogeneous boundary conditions, the solutions to the fractional Poisson equation are continuous but not continuously differentiable across the boundary[37]. This reduces the convergence rates of many numerical methods. Thirdly, the memory and computational cost of the fractional partial differential equations is in general higher than its integer-order counterpart since the resultant linear system is usually dense. In sum, for the fractional partial differential equations involving the fractional Laplacian to be practical, designing an easy-to-implement, accurate and efficient numerical method is desirable.

Many existing methods suffer from their applicability or numerical issues. For example, [43] proposed a radial basis function collocation method for decoupled fractional Laplacian wave equations. The resultant linear system is usually ill-conditioned due to its meshless nature. [29] proposed a “walk-on-spheres” Monte Carlo methods for the fractional Laplacian. The method requires a large number of simulations, especially for small s , where the “jump size” is very large and thus the variance is large. [42] proposed a spectral method for 2D and 3D but the method is only limited to the unit ball domains.

Since the seminal paper by Hughes et al. [26], there has been extensive research on the isogeometric analysis. The basic idea is to use the same NURBS-based representation for both the solution and the geometry. By doing so, the isogeometric analysis can represent many complex geometries exactly. Additionally, the parametrized solution has high-order continuous derivatives depending on the choice of the NURBS basis functions, which enables us to work directly with the strong form of the fractional Laplacian.

This inspired us to attack the computational challenges in nonlocal models involving the fractional Laplacian with the isogeometric collocation method. Compared to the finite element analysis [2, 3], the isogeometric collocation method is much easier to implement and we show that our method is more accurate per degree of freedom than the finite element analysis due to its smooth basis functions. Compared to methods such as finite difference methods [25, 32], isogeometric analysis enables representing various geometrical shapes exactly such as a disk. Isogeometric analysis offers a new way to solve the fractional differential equations and can be generalized to other nonlocal models.

The article is organized as follows. In Section 2, we describe the isogeometric collocation method. In Section 3, we propose an algorithm for solving the fractional Poisson problem based on the isogeometric collocation method, where we construct the interpolation matrix and the discrete fractional Laplacian matrix. In Section 4 we perform the numerical benchmarks on generalized eigenvalues and eigenfunctions of the fractional Laplacian operator. We are able to compare the numerical solutions with analytical solutions and access convergence rates. Specifically, we compare the accuracy of the proposed method with the finite element method on a per-degree-of-freedom basis. We also consider the application of our method to the fractional porous media equation. The numerical results show the potential of isogeometric analysis for solving nonlocal models. We discuss the limitations and future research directions in Section 5.

For reference, we list all notation used in this paper in Table 1. The codes for this work will be available at <https://github.com/kailaix/IGA.jl>.

Notation	Description
s	the fractional index
$c_{s,2}$	the normalization constant in the fractional Laplacian
$(-\Delta)^s$	the fractional Laplacian
$B_{i,p}$	the B-spline basis function
$N_{i,j}$	the NURBS basis function
\mathcal{C}^k	the function space with up to k -th order continuous derivatives
w_i	weights associated with the NURBS basis functions
$\tilde{\mathbf{X}}_i, \tilde{\mathbf{X}}_{ij}$	control points in 1D and 2D
F, \mathbf{F}	mapping from the parameter space to the physical space
\mathbf{V}	the interpolation function space defined by the NURBS basis functions
$\hat{\mathbf{u}}_{ij}, \hat{\mathbf{x}}_{ij}$	the collocation points in the parameter and physical space
ρ, a	the window function and the window size
$(-\Delta)_h ((-\Delta)_h^s)$	the discrete (fractional) Laplacian
\mathbf{M}	the interpolation matrix
\mathbf{L}	the discrete fractional Laplacian matrix

Table 1: Notation used in this paper

2. Isogeometric Collocation Method

In isogeometric analysis, the basis functions for approximating the solutions are non-uniform rational basis splines (NURBS). These basis functions emanate from computer-aided geometric design (CAGD) in contrast to the Lagrange finite element interpolation polynomials used in finite element analysis [39]. In this section, we present an overview of the isogeometric collocation method. For details on isogeometric analysis, see the appendix.

Consider the generalized boundary-value problem

$$\mathcal{L}u = f \text{ in } \Omega, \quad u = 0 \text{ in } \Omega^c \quad (4)$$

where the solution $u : \mathbb{R}^2 \rightarrow \mathbb{R}$ has a compact support in Ω and \mathcal{L} is the fractional Laplacian, i.e., $(-\Delta)^s$. f is the source term.

We introduce a NURBS representation of Ω . The collocation points are comprised of a finite set in the parameter space $\{\hat{\mathbf{u}}_i\}_{i \in \mathcal{I}}$, where $\mathcal{I} = \mathcal{I}_D \cup \mathcal{I}_L$ is divided into two distinct sets [5]. The points in \mathcal{I}_D lie on $\partial\Omega$ while those in \mathcal{I}_L are inside Ω . Then, the isogeometric collocation method finds $u_h \in \mathbf{V}$ such that

$$\mathcal{L}u_h(\mathbf{F}(\hat{\mathbf{u}}_i)) = f(\mathbf{F}(\hat{\mathbf{u}}_i)) \quad i \in \mathcal{I}_L \quad (5)$$

$$u_h(\mathbf{F}(\hat{\mathbf{u}}_i)) = 0 \quad i \in \mathcal{I}_D \quad (6)$$

A commonly used set of collocation points is derived from the Greville abscissae [27]. The Greville abscissae \bar{u}_i are related to the knot vector $\{u_1, u_2, \dots, u_{l+1}\}$ by

$$\bar{u}_i = \frac{u_{i+1} + u_{i+2} + \dots + u_{i+p}}{p} \quad (7)$$

Analogously, in two dimension, we can construct the Greville abscissae \bar{u}_i, \bar{v}_j for both dimensions and consider the tensor product

$$\hat{\mathbf{u}}_{ij} = (\bar{u}_i, \bar{v}_j) \quad \hat{\mathbf{x}}_{ij} = \mathbf{F}(\hat{\mathbf{u}}_{ij})$$

Then the isogeometric analysis collocation method reads: find $u_h \in \mathbf{V}$ such that

$$\begin{aligned} \mathcal{L}u_h(\hat{\mathbf{x}}_{ij}) &= f(\hat{\mathbf{x}}_{ij}) & i = 2, 3, \dots, l_u - p - 1; j = 2, 3, \dots, l_v - q - 1 \\ u_h(\hat{\mathbf{x}}_{ij}) &= 0 & (i, j) \in \{1, l_u - p\} \times \{1, 2, \dots, l_v - q\} \cup \{1, 2, \dots, l_u - p\} \times \{1, l_v - q\} \end{aligned}$$

3. Numerical Scheme

3.1. Singularity Subtraction

In this section, we will consider the discretization of the fractional Laplacian operator. Assume the knot vectors for u and v are

$$\{u_1, u_2, \dots, u_{l_u+1}\} \quad \{v_1, v_2, \dots, v_{l_v+1}\}$$

and the degrees are p and q respectively. Let $\hat{\mathbf{u}}_{ij}$ be the collocation points derived from the Greville abscissae, and $\hat{\mathbf{x}}_{ij} = \mathbf{F}(\hat{\mathbf{u}}_{ij})$.

Assume that $u(\mathbf{x}) \in \mathcal{C}^4$, we compute the principal value integral

$$\text{p.v.} \int_{\mathbb{R}^2} \frac{u(\mathbf{x}) - u(\mathbf{y})}{|\mathbf{x} - \mathbf{y}|^{2+2s}}$$

using the singularity subtraction method [32]

$$\int_{\mathbb{R}^2} \frac{u(\mathbf{x}) - u(\mathbf{y})}{|\mathbf{x} - \mathbf{y}|^{2+2s}} d\mathbf{y} = \int_{\mathbb{R}^2} \frac{u(\mathbf{x}) - u(\mathbf{y}) + \rho(|\mathbf{x} - \mathbf{y}|)g_{\mathbf{x}}(\mathbf{y})}{|\mathbf{x} - \mathbf{y}|^{2+2s}} d\mathbf{y} - \int_{\mathbb{R}^2} \frac{\rho(|\mathbf{x} - \mathbf{y}|)g_{\mathbf{x}}(\mathbf{y})}{|\mathbf{x} - \mathbf{y}|^{2+2s}} d\mathbf{y} \quad (8)$$

where ρ is a window function defined by

$$\rho(r) = \begin{cases} 1 - 35 \left(\frac{r}{a}\right)^4 + 84 \left(\frac{r}{a}\right)^5 - 70 \left(\frac{r}{a}\right)^6 + 20 \left(\frac{r}{a}\right)^7 & r < a \\ 0 & \text{otherwise} \end{cases} \quad (9)$$

Here $a > 0$ is the window size and $g_{\mathbf{x}}(\mathbf{y})$ is the truncated Taylor expansion of $u(\mathbf{y}) - u(\mathbf{x})$

$$\begin{aligned} g_{\mathbf{x}}(\mathbf{y}) &:= u_1(\mathbf{x})v_1 + u_2(\mathbf{x})v_2 \\ &+ u_{11}(\mathbf{x})\frac{v_1^2}{2} + u_{22}(\mathbf{x})\frac{v_2^2}{2} + u_{12}(\mathbf{x})v_1v_2 \\ &+ u_{111}(\mathbf{x})\frac{v_1^3}{6} + u_{112}(\mathbf{x})\frac{v_1^2v_2}{2} + u_{122}(\mathbf{x})\frac{v_1v_2^2}{2} + u_{222}(\mathbf{x})\frac{v_2^3}{6} \end{aligned} \quad (10)$$

Here we have used the abbreviation for the derivatives of $\mathbf{v} = (v_1, v_2) = \mathbf{y} - \mathbf{x}$,

$$u_i := \frac{\partial u}{\partial \mathbf{x}_i}, \quad u_{ij} := \frac{\partial^2 u}{\partial \mathbf{x}_{ij}^2}, \quad u_{ijk} := \frac{\partial^3 u}{\partial \mathbf{x}_{ijk}^3}, \quad i, j, k \in \{1, 2\}$$

The function ρ was chosen such that $\rho(r) = 1 + \mathcal{O}(r^4)$, $r \rightarrow 0+$, $u(\mathbf{x}) - u(\mathbf{y}) + \rho(|\mathbf{x} - \mathbf{y}|)g_{\mathbf{x}}(\mathbf{y}) \sim \mathcal{O}(|\mathbf{x} - \mathbf{y}|^4)$, $\mathbf{y} \rightarrow \mathbf{x}$, so that the integrand in

$$\int_{\mathbb{R}^2} \frac{u(\mathbf{x}) - u(\mathbf{y}) + \rho(|\mathbf{x} - \mathbf{y}|)g_{\mathbf{x}}(\mathbf{y})}{|\mathbf{x} - \mathbf{y}|^{2+2s}} d\mathbf{y} \quad (11)$$

is continuous, and thus integrable. Figure 1 shows $\frac{u(\mathbf{x}) - u(\mathbf{y}) + \rho(|\mathbf{x} - \mathbf{y}|)g_{\mathbf{x}}(\mathbf{y})}{|\mathbf{x} - \mathbf{y}|^{2+2s}}$ and $\frac{|u(\mathbf{x}) - u(\mathbf{y})|}{|\mathbf{x} - \mathbf{y}|^{2+2s}}$ for $s = 0.3$. We can see that by singularity subtraction, the integrand is turned into a continuous function suitable for a standard numerical quadrature rule. The window function is shown in Figure 2.

Due to symmetry, the second part of Eq. (8) is

$$\int_{\mathbb{R}^2} \frac{\rho(|\mathbf{x} - \mathbf{y}|)g_{\mathbf{x}}(\mathbf{y})}{|\mathbf{x} - \mathbf{y}|^{2+2s}} d\mathbf{y} = \frac{1}{2} \Delta u(\mathbf{x}) \int_{\mathbb{R}^2} \frac{\rho(|\mathbf{y}|)\mathbf{y}_1^2}{|\mathbf{y}|^{2+2s}} d\mathbf{y} \quad (12)$$

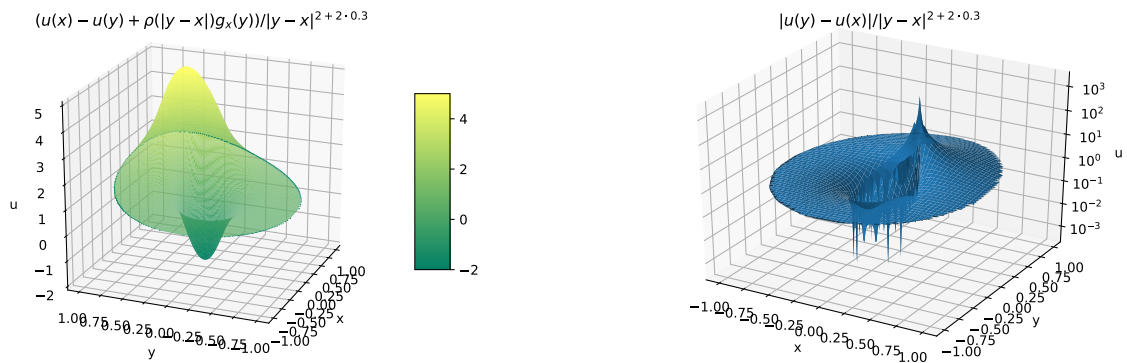


Figure 1: $\frac{u(\mathbf{x}) - u(\mathbf{y}) + \rho(|\mathbf{x} - \mathbf{y}|)g_{\mathbf{x}}(\mathbf{y})}{|\mathbf{x} - \mathbf{y}|^{2+2s}}$ and $\frac{|u(\mathbf{x}) - u(\mathbf{y})|}{|\mathbf{x} - \mathbf{y}|^{2+2s}}$ for $s = 0.3$ and $u(\mathbf{x}) = (1 - |\mathbf{x}|^2)^{1+s}$. The function on the left is continuous while the one on the right has a singularity. By singularity subtraction, the integrand is turned into a continuous function suitable for a standard numerical quadrature rule. Note that the derivative of the integrand is not necessarily continuous.

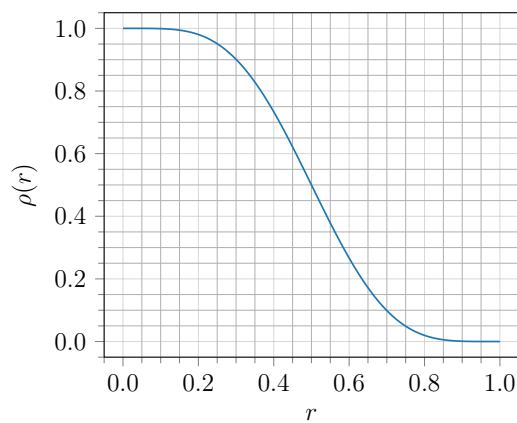


Figure 2: An example of the window function Eq. (9) for $a = 1$. The function behaves like $1 - \mathcal{O}(r^4)$ near the origin.

3.2. Numerical Discretization

We now adopt a standard numerical quadrature rule for computing Eq. (11). The idea is that for a function in 2D we can express it in the polar coordinates

$$\int_{\mathbb{R}^2} f(\mathbf{x}) d\mathbf{x} = \int_0^\infty dr \int_{\mathbb{S}^1} r f(r\boldsymbol{\sigma}) d\boldsymbol{\sigma} \quad (13)$$

where \mathbb{S}^1 is the unit circle. The numerical quadrature is constructed from the tensor product of the Gauss Legendre quadrature rule in the radial direction and the trapezoidal rule in the axial direction, i.e.,

$$\boldsymbol{\xi}_{ij} = r_i \boldsymbol{\sigma}_j, \quad w_{ij}^Q = \frac{2\pi w_j^{GL} r_i}{m}, \quad i = 1, 2, \dots, n; \quad j = 1, 2, \dots, m \quad (14)$$

where (r_i, w_{ij}^{GL}) are Gauss Legendre quadrature points and weights in $[0, R]$ for a sufficient large R . Therefore, Eq. (11) can then be discretized as

$$\sum_{i=1}^n \sum_{j=1}^m \frac{2\pi w_{ij}^{GL}}{m} \frac{u(\mathbf{x}) - u(\mathbf{x} + \boldsymbol{\xi}_{ij}) + \frac{\rho_i r_i^2 \Delta u(\mathbf{x})}{2}}{r_i^{1+2s}}$$

here $\rho_i = \rho(r_i)$. For the Laplacian operator Δ , we consider the fourth order discretization [16]

$$\Delta u(\mathbf{x}) \approx \Delta_h u(\mathbf{x}) = \sum_{i=1}^2 \frac{-\frac{1}{12}u(\mathbf{x} - 2\mathbf{e}_i h) + \frac{4}{3}u(\mathbf{x} - \mathbf{e}_i h) - \frac{5}{2}u(\mathbf{x}) + \frac{4}{3}u(\mathbf{x} + \mathbf{e}_i h) - \frac{1}{12}u(\mathbf{x} + 2\mathbf{e}_i h)}{h^2} \quad (15)$$

here $\mathbf{e}_1 = \begin{bmatrix} 1 \\ 0 \end{bmatrix}$, $\mathbf{e}_2 = \begin{bmatrix} 0 \\ 1 \end{bmatrix}$. Note we require $u(\mathbf{x}) \in \mathcal{C}^4$ to obtain the fourth order estimate of the discretization Eq. (15).

Define

$$A = 2\pi \sum_{i=1}^n \frac{w_{ij}^{GL}}{r_i^{1+2s}}, \quad B = \sum_{i=1}^n \frac{\pi w_{ij}^{GL} \rho_i}{r_i^{2s-1}} - \pi \int_0^a \frac{\rho(r)}{r^{2s-1}} dr$$

then the discretization of the fractional Laplacian operator is given as

$$(-\Delta)^s u(\mathbf{x}) \approx (-\Delta)_h^s u(\mathbf{x}) = c_{s,2} \left(Au(\mathbf{x}) - \sum_{i=1}^n \sum_{j=1}^m \frac{2\pi w_{ij}^{GL}}{m r_i^{1+2s}} u(\mathbf{x} + \boldsymbol{\xi}_{ij}) + B \Delta_h u(\mathbf{x}) \right) \quad (16)$$

We pick a sufficient large R so that the computational domain Ω is contained in the convex hull of the numerical quadrature points. Only the terms such that $\mathbf{x} + \boldsymbol{\xi}_{ij} \in \Omega$ do not vanish in the second summation Eq. (16). Figure 3 depicts such an example where Ω is the unit disk and $\mathbf{x} + \boldsymbol{\xi}_{ij}$ corresponds to the non-vanishing terms for two \mathbf{x} 's are shown.

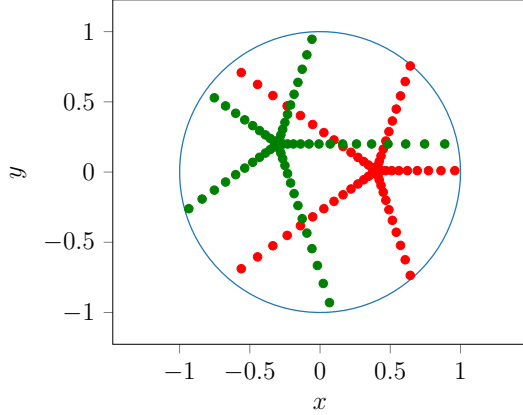


Figure 3: An example of quadrature points used in evaluating the second term in Eq. (16).

3.3. Interpolation Matrix and the Discrete Fractional Laplacian Matrix

Let us consider any point $\mathbf{x} \in \Omega$, then there exists $\mathbf{u} = \begin{bmatrix} u \\ v \end{bmatrix}$ in the parameter space such that $\mathbf{F}(\mathbf{u}) = \mathbf{x}$. The numerical solution $u_h \in \mathbf{V}$ can be written as

$$u_h(\mathbf{x}) = u_h(\mathbf{F}^{-1}(\mathbf{u})) := \sum_{i=1}^{l_u-p} \sum_{j=1}^{l_v-q} N_{i,j}(u, v) c_{ij} \quad (17)$$

Since every NURBS basis function only spans pq patches in the parameter space, no more than pq terms in the summation in Eq. (17) are nonzero. If \mathbf{x} are the collocation points derived from Greville abscissae, we have

$$u_h(\hat{\mathbf{x}}) = \mathbf{M}\mathbf{c} \quad (18)$$

where $\hat{\mathbf{x}} = \text{vec}(\{\hat{\mathbf{x}}_{ij}\}_{i=1,2,\dots,l_u-p; j=1,2,\dots,l_v-q})$, $\mathbf{c} = \text{vec}(\{c_{ij}\})$ and \mathbf{M} is a sparse matrix with at most pq non-zeros per row. Here vec is the vectorization of a matrix,

$$\text{vec}(\{\mathbf{x}_{ij}\}_{ij}) = [\mathbf{x}_{11}, \dots, \mathbf{x}_{l_u-p,1}, \mathbf{x}_{12}, \dots, \mathbf{x}_{l_u-p,2}, \dots, \mathbf{x}_{1,l_v-q}, \dots, \mathbf{x}_{l_u-p,l_v-q}]^T$$

We call \mathbf{M} the *interpolation matrix*, which maps the coefficients from the parameter space to pointwise values in the physical space and vice versa.

To compute Eq. (16), assume that $u(\mathbf{x})$ is given in terms of the coefficients \mathbf{c} in the parameter space, then we can evaluate the values of u at \mathbf{x} , $\mathbf{x} + \boldsymbol{\xi}_{ij}$, $\mathbf{x} \pm h\mathbf{e}_i$, and $\mathbf{x} \pm 2h\mathbf{e}_i$ using Eq. (17). The values are computed and plugged into Eq. (16) to obtain the values $(-\Delta)_h^s u(\mathbf{x})$, which is linear in the coefficients \mathbf{c} . If the collocation points are $\{\hat{\mathbf{x}}_{ij}\}$, we denote the associated linear operator that can be expressed by a matrix \mathbf{L} , and then we have

$$(-\Delta)_h^s u(\hat{\mathbf{x}}) = \mathbf{L}\mathbf{c} \quad (19)$$

The interpolation matrix \mathbf{M} and the discrete fractional Laplacian matrix \mathbf{L} can be pre-computed. Algorithm 1 shows the algorithm for solving the Poisson equation using the matrices \mathbf{M} and \mathbf{L} mentioned above.

Algorithm 1 Solving the fractional Poisson problem using the interpolation matrix and the discrete fractional Laplacian matrix.

- 1: **Input:** f **Output:** $u_h(\hat{\mathbf{x}}_{ij})$
 - 2: Precompute \mathbf{L}, \mathbf{M}
 - 3: $\mathbf{f} \leftarrow \text{vec}(\{\mathbf{f}_{ij}\}_{ij})$ where $\mathbf{f}_{ij} = f(\hat{\mathbf{x}}_{ij})$
 - 4: $\mathbf{f}[\mathcal{I}_D] \leftarrow 0$ {Recall that \mathcal{I}_D are the degrees of freedom associated with boundaries.}

 - 5: $\mathbf{L}[\mathcal{I}_D, :] = \mathbf{M}[\mathcal{I}_D, :]$ {Impose the zero boundary conditions.}
 - 6: $\mathbf{c} \leftarrow \mathbf{L}^{-1}\mathbf{f}$
 - 7: **return** $\mathbf{M}\mathbf{c}$
-

3.4. Convergence and Error Bounds

The choice m and n in the numerical quadrature rule Eq. (14) as well the choice of step size h in Eq. (15) affects the accuracy of the numerical scheme. As we show in the numerical examples, these parameters will influence the accuracy while having little impact on the convergence rate.

The approximation ability depends on the number of knots, the degrees, and the mesh structure of the NURBS surface. It is shown that under appropriate assumptions, the NURBS space on the physical domain delivers the optimal rate of the convergence, similar to the finite element space of degree p [6]. The following lemma gives the global error estimate

Lemma 1. *Let k and l be integer indices with $0 \leq k \leq l \leq p + 1$, we have*

$$\sum_{K \in \mathcal{K}_h} \|v - \Pi_{\mathcal{V}_h} v\|_{\mathcal{H}_h^k(K)}^2 \leq C_{\text{shape}} \sum_{K \in \mathcal{K}_h} h_K^{2(l-k)} \sum_{i=0}^l \|\nabla F\|_{L^\infty(F^{-1}(K))}^{2(i-l)} |v|_{H^i(K)}^2 \quad \forall v \in H^l(\Omega)$$

For the proof the readers are referred to [6]. Here \mathcal{K}_h are the patches in the parametric space, \mathcal{V}_h is the NURBS space, C_{shape} is a constant depending on the structure of the NURBS surface, H^i is the standard Sobolev space, h_K is the diameter of K , and $\mathcal{H}_h^k(K)$ are patches in the physical space endowed with its own norms. The lemma indicates that if v is sufficiently smooth, increasing the degree of the NURBS surface (p -refinement) or the number of control points (h -refinement) will yield better approximations. However, it may not be the case for less smooth functions, where are often encountered in the PDEs involving the fractional Laplacian [37].

We assume that the domain Ω satisfies the exterior ball condition, i.e., there exists a positive radius ρ_0 such that all the points on $\partial\Omega$ can be touched by some exterior ball of radius ρ_0 . The solution to the fractional Poisson equation (Eq. (4)) with $\mathcal{L} = (-\Delta)^s$ is only Hölder continuous according to Corollary 1.6 in [37].

Lemma 2. *Let Ω be a bounded $C^{1,1}$ domain satisfying the exterior ball condition, $f \in L^\infty(\Omega)$, u be a solution of Eq. (4) with $\mathcal{L} = (-\Delta)^s$. Then,*

$$u \in C^{0,s}(\mathbb{R}^2) \quad \text{and} \quad \|u\|_{C^{0,s}} \leq C \|f\|_{L^\infty(\Omega)}$$

where C is a constant depending only on Ω and s .

The lemma indicates that the solution is Hölder continuous. In fact, it is also shown in [37] that $\frac{u}{\delta^s}$ is continuous in $\bar{\Omega}$, i.e., the solution is continuous but not continuously differentiable near the boundary. For the case $s > \frac{1}{2}$, we have the following estimate

Theorem 1. *Assume that Ω is a bounded $C^{1,1}$ domain satisfying the exterior ball condition, $f \in L^\infty(\Omega)$, u be a solution of Eq. (4) with $\mathcal{L} = (-\Delta)^s$, $s > \frac{1}{2}$. In addition, assume that the mesh is quasi-uniform, i.e., there exists $\gamma_1 \leq 1 \leq \gamma_2$, such that*

$$\gamma_1 h \leq h_K \leq \gamma_2 h \quad \forall K \in \mathcal{K}_h \quad (20)$$

then there exists $C > 0$ such that

$$\sum_{K \in \mathcal{K}_h} \|u - \Pi_{\mathcal{V}_h} u\|_{L^2(\Omega)}^2 \lesssim h^2 \quad (21)$$

To prove Theorem 1, we need the following embedding lemma [1]

Lemma 3. *Assume that Ω is a bounded $C^{1,1}$ domain, $m, k \in \mathbb{N}_0$, $p \in [1, \infty)$, $\alpha \in [0, 1]$.*

$$m - \frac{n}{p} \leq k + \alpha \quad \alpha \neq 0, 1 \quad (22)$$

then $W^{m,p}(\Omega) \subset C^{k,\alpha}(\bar{\Omega})$ and there is a constant $C > 0$, s.t.

$$\|u\|_{W^{m,p}(\Omega)} \leq C \|u\|_{C^{k,\alpha}(\Omega)} \quad (23)$$

If $m - \frac{n}{p} < k + \alpha$, the embedding is compact.

Proof of Theorem 1. Due to Lemma 2, the solution is s -Hölder continuous. Let $n = p = 2$, $m = 1$, $k = 0$, $\alpha = s$ in Lemma 3, we have

$$\|u\|_{H^1} \leq C \|u\|_{C^{0,s}(\Omega)}$$

for a constant $C > 0$. We invoke Lemma 1 with $l = 1$, $k = 0$, and thus have

$$\sum_{K \in \mathcal{K}_h} \|u - \Pi_{\mathcal{V}_h} u\|_{L^2(\Omega)}^2 \lesssim h^2$$

□

Note for the case $s \leq \frac{1}{2}$ the proof is not applicable. Nevertheless, we observe numerically that we obtain the $\mathcal{O}(h^2)$ convergence rate.

Another source of error is the numerical error of solving the linear system $\mathbf{L}\mathbf{c} = \mathbf{f}$ in Algorithm 1. The condition number of \mathbf{L} grows as we increase the number of control points. The convergence of the iterative solver such as GMRES may be slow if no proper preconditioner is used. In fact, it is shown that for finite element methods, if a family of shape regular and globally quasi-uniform triangulations with maximal element size h is used, the stiffness matrix satisfies [4]

$$\kappa(\mathbf{L}) = Ch^{-2s}$$

In the paper, we have used Greville abscissae as the collocation points, which have been widely adopted as the default choice in the isogeometric analysis literature [36].

4. Numerical Experiments

4.1. Numerical Benchmark

For verification and benchmarking we consider the generalized eigenvalue problem for $(-\Delta)^s$ in a unit disk $\Omega \subset \mathbb{R}^d$, with a zero condition in the complement of Ω

$$\begin{cases} (-\Delta)^s ((1 - |\mathbf{x}|^2)^s \varphi_n(\mathbf{x})) = \lambda_n \varphi_n(\mathbf{x}) & \mathbf{x} \in \Omega \\ \varphi_n(\mathbf{x}) = 0 & \mathbf{x} \notin \Omega \end{cases} \quad (24)$$

where $n = 0, 1, \dots$. The eigenvalues λ_n and the eigenfunctions $\varphi_n(\mathbf{x})$ are given as [13]

$$\lambda_n = \frac{2^{2s} \Gamma(s + n + 1)^2}{(n!)^2} \quad \varphi_n(\mathbf{x}) = (-1)^n P_n^{(s,0)}(2|\mathbf{x}|^2 - 1)$$

We assume the right hand side $\lambda_n \varphi_n(\mathbf{x})$ is given and we apply the proposed algorithm Algorithm 1 to obtain the numerical solution $u_h(\hat{\mathbf{x}}_{ij})$. The error is computed using

$$\text{error} = \sqrt{\frac{\sum_{i,j} |u_h(\hat{\mathbf{x}}_{ij}) - (1 - |\hat{\mathbf{x}}_{ij}|^2)^s \varphi_n(\hat{\mathbf{x}}_{ij})|^2}{(l_u - p)(l_v - q)}} \quad (25)$$

here $(1 - |\hat{\mathbf{x}}_k|^2)^s \varphi_n(\hat{\mathbf{x}}_k)$ is the exact solution at $\hat{\mathbf{x}}_k$.

The numerical experiments are carried out with parameters $s = 0.8$, $a = 0.1$, $h = 0.001$, $R = 20$, $p = q = 2$, $n = 1, 2, 3, 4, 5$. In the first case we use $m = 20$, $n = 1000$ while in the second case we use $m = 40$, $n = 5000$ (m and n are the number of quadrature points in the axial and radial directions). Figure 4 shows the convergence results for Eq. (24). The first column shows the reference solution. The second column shows the convergence of the algorithm with respect the degrees of freedom N by varying the number of refinements for different number of quadrature points. We have obtained monotonous convergence and observed $\mathcal{O}(N^{-1})$ convergence for all cases, where N is the degrees of freedom. m and n influence the final error while having little impact on the convergence order. Larger numbers of quadrature points yield more accurate results.

Note that the exact solutions $(1 - |\mathbf{x}|^2)^s \varphi_n(\mathbf{x})$ are continuous but not \mathcal{C}^1 on the boundary $|\mathbf{x}| = 1$. However, we observe no difficulty in applying the proposed algorithm even though we have required \mathcal{C}^3 for the singularity subtraction and \mathcal{C}^4 for the fourth-order discretization of the Laplacian operator. This is because the collocation points derived from the Greville abscissae are usually denser near the boundary and therefore mitigate accuracy loss partially.

4.2. Comparison with FEM

In this section, we compare the accuracy of the proposed algorithm with finite element analysis on a per-degree-of-freedom basis. We solve the same problem in Eq. (24) with $n = 2$ and $s = 0.5$ using isogeometric analysis as well as finite element analysis [2]. The corresponding finite element analysis codes are made available by the authors.¹ For the

¹We used the codes from

<https://github.com/fbersetche/A-short-FE-implementation-for-a-2d-homogeneous-Dirichlet-problem-of-a-Fractional-Laplacian>

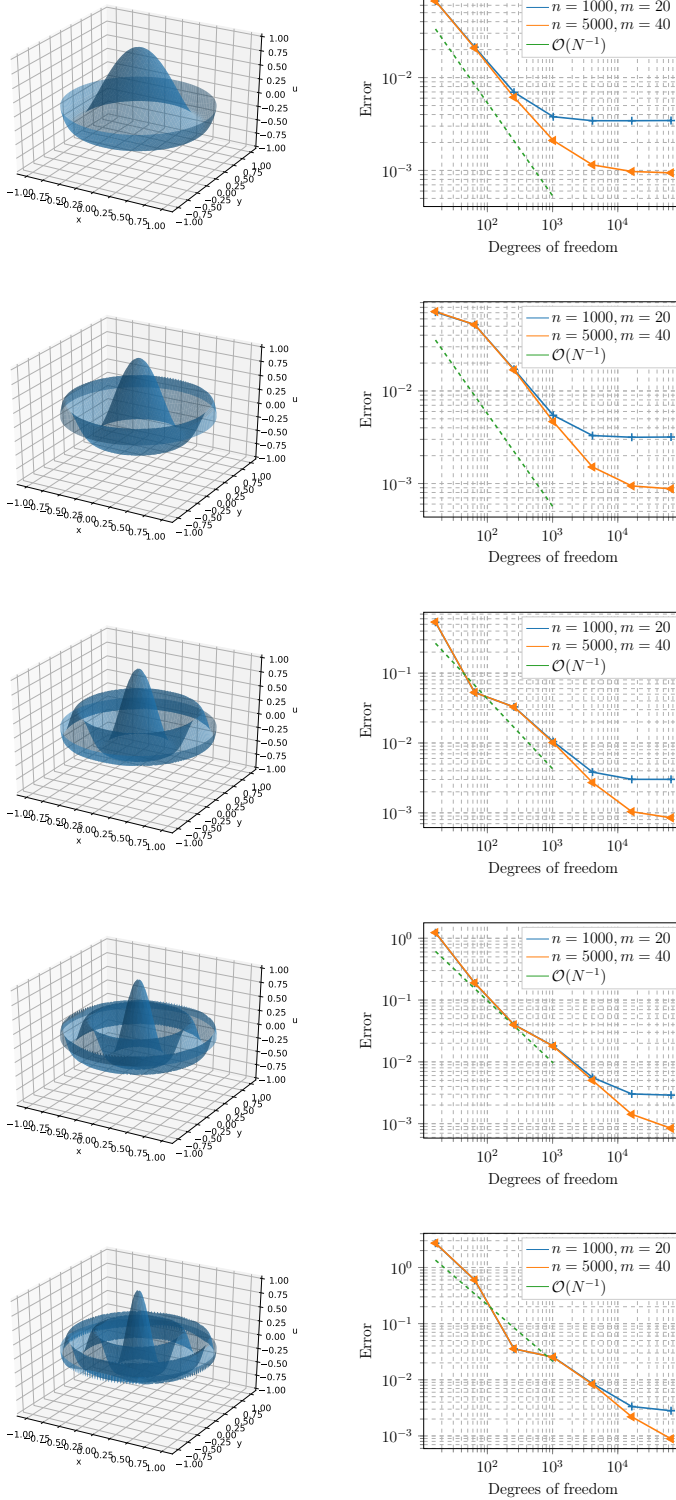


Figure 4: Convergence results for Eq. (24). The first column shows the reference solution. The second column shows the convergence of the algorithm with respect the degrees of freedom N by varying the number of refinements for different number of quadrature points. The parameters m and n are the number of quadrature points in the axial and radial directions.

finite element method, the error is measured as the mean squared error on the vertices $\tilde{\mathbf{x}}_k$ of the mesh triangles, i.e.

$$\text{error} = \sqrt{\frac{\sum_k |u_h(\mathbf{x}_k) - (1 - |\mathbf{x}_k|^2)^s \varphi_n(\mathbf{x}_k)|^2}{(l_u - p)(l_v - q)}}$$

In Figure 5, we report the log-scale plots of the errors for FEM and isogeometric analysis (IGA) with $n = 1000$, $m = 20$ and $n = 5000$, $m = 40$. We can see that isogeometric analysis exhibits superior accuracy compared with finite element analysis for the fractional Laplacian problem. Besides, isogeometric analysis yields a better convergence rate without particular preprocessing such as the graded meshes adopted in [2]. We also point out the isogeometric analysis code is much easier to implement, while for finite element analysis we need to carefully treat the quadrature rules for the singular kernel. For example, [2] applied the Duffy-type transforms and implemented different quadrature rules according to the relative position of two triangle elements (i.e., identical, sharing a vertex, sharing an edge and disjoint).

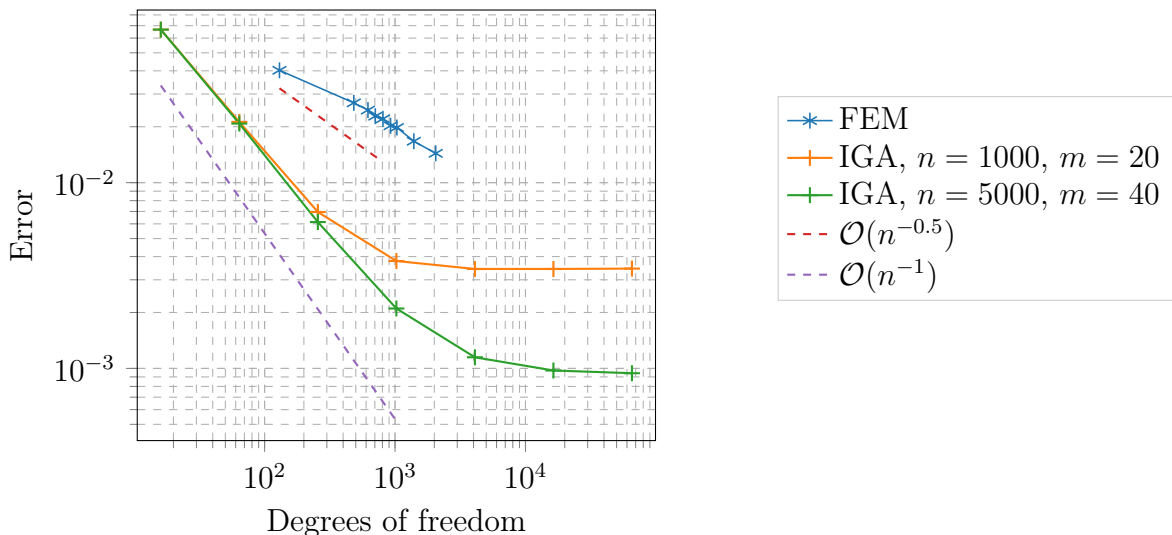


Figure 5: Isogeometric analysis exhibits superior accuracy compared with finite element analysis for the fractional Laplacian problem.

4.3. Application: Porous Medium Equation with the Fractional Laplacian

This application is concerned with the fractional porous media equation, which describes anomalous diffusion in the porous media [12]

$$\begin{cases} u_t + (-\Delta)^s(|u|^{m-1}u) = 0 & \mathbf{x} \in \mathbb{R}^2, t > 0 \\ u(\mathbf{x}, 0) = f(\mathbf{x}) & \mathbf{x} \in \mathbb{R}^2 \end{cases} \quad (26)$$

The motivation of studying nonlocal models for diffusion in porous media is two folds: on the one hand, the traditional diffusion equation which leads to a Gaussian solution does

not always agree with experimental results, and in some cases fractional models are required to match experiments; on the other hand, the fractional diffusion equation Eq. (26) can be derived from “first principle” using statistical mechanics, i.e., the fractional Laplacian naturally arises from macroscopic governing equations of particles undergoing α -stable Lévy motion. The associated parameter s can be found from experimental data [18, 31, 41]. In sum, the use of fractional Laplacian operator leads to more accurate modeling compared to integer-order differential equation approximations.

We truncate the domain to $[-1, 1]^2$ and only consider the nonnegative solutions $u \geq 0$. Define $t_n = (n - 1)\Delta t$ to be the integration time $0 \leq t_n \leq T$ and $\Delta t = \frac{T}{n_T}$. Let u_{ij}^n be the numerical solution to $u(\hat{\mathbf{x}}_{ij}, t_n)$ and denote $\mathbf{u}^n = \text{vec}(\{u_{ij}^n\}_{ij})$. We denote $(u^m)_{ij}^n = u(\hat{\mathbf{x}}_{ij}, t_n)^m$. Consider the Crank-Nicolson discretization for Eq. (26)

$$\frac{u_{ij}^{n+1} - u_{ij}^n}{\Delta t} + \frac{1}{2}(-\Delta)^s (u^m)_{ij}^{n+1} + \frac{1}{2}(-\Delta)^s (u^m)_{ij}^n = 0$$

To linearize the equation, we consider the same technique used in [35]

$$(u^m)_{ij}^{n+1} \approx (u^m)_{ij}^n + m(u^{m-1})_{ij}^n (u_{ij}^n - u_{ij}^{n-1})$$

Using the matrices in Section 3.3, we have the discretized equation (assuming $\mathbf{u}^{-1} = \mathbf{0}$)

$$\begin{aligned} \mathbf{u}^{n+1} &= \mathbf{u}^n - \frac{m\Delta t}{2} \mathbf{F}^* \mathbf{M}^{*-1} ((\mathbf{u}^{m-1})^n \otimes (\mathbf{u}^n - \mathbf{u}^{n-1})) - \frac{\Delta t}{2} \mathbf{F}^* \mathbf{M}^{*-1} (\mathbf{u}^m)^n \quad n = 1, 2, \dots, n_T \\ \mathbf{u}^1 &= \mathbf{f} \end{aligned}$$

where $\mathbf{f} = \text{vec}(\{f(\hat{\mathbf{x}}_{ij})\}_{i,j \in \mathcal{I}_L})$, and \otimes denotes the element-wise multiplication, and

$$\mathbf{M}^* = \mathbf{M}[\mathcal{I}_L, \mathcal{I}_L] \quad \mathbf{L}^* = \mathbf{L}[\mathcal{I}_L, \mathcal{I}_L]$$

In the numerical example, we let $f(\mathbf{x}) = \exp(-100|\mathbf{x}|^2)$, $a = 0.1$, $R = 20$, $h = 1000$, $n_T = 1000$, $\Delta t = 0.0001$, 1000 quadrature points in the radial direction and 20 in the axial direction. Figure 6 shows the changes in the value $u_h(\mathbf{0}, t)$ for $0 \leq t \leq 0.1$ and different m , s . Typically we do not have analytical solutions for general m and s ; however, in the special case when $m = 1$ and $s = 0.5$, we obtain the equation

$$\frac{\partial u}{\partial t} + (-\Delta)^{1/2} u = 0$$

the linear fractional heat equation has analytical solution through convolution with the explicit Poisson kernel in \mathbb{R}_+^3 (\mathbb{R}^2 spatial and \mathbb{R}_+ temporal) [12]

$$u(\mathbf{x}, t) = c_{1/2,2} \int_{\mathbb{R}^2} \frac{tf(\mathbf{y})}{(|\mathbf{x} - \mathbf{y}|^2 + t^2)^{3/2}} d\mathbf{y}$$

Particularly, we have in our case

$$u(\mathbf{0}, t) = 1 - 10\sqrt{\pi t^2} e^{100t^2} \text{erfc}(10t) \tag{27}$$

The equation Eq. (27) can be used for verification and the values are plotted alongside the numerical results in Figure 6. We can see that the numerical result and the exact solution coincide for $t \in [0, 0.1]$ and $s = 0.2, m = 1$. We can also see that the larger the s or the smaller the m , the faster the diffusion is. Different values of s and m provide different profiles of the diffusion process and therefore form a powerful tool for modeling anomalous diffusion. Figure 7 shows the diffusion profile at $t = 0.1$ for different cases.

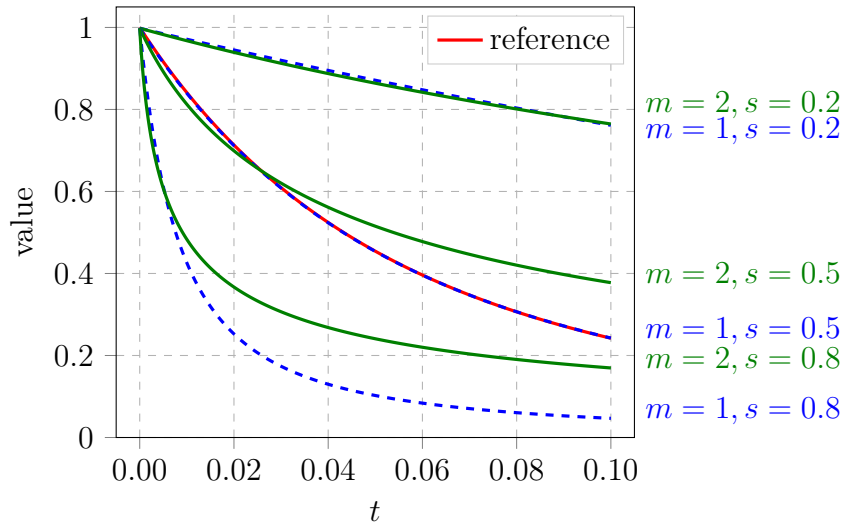


Figure 6: Evolution of $u_h(\mathbf{0}, t)$ in different settings. The numerical results coincide with the exact solution for $m = 1, s = 0.5$. The reference solution is given only for $m = 1, s = 0.5$, because analytical solutions are not available for the other parameters.

5. Conclusion

We have studied the NURBS-based isogeometric analysis for PDEs involving the fractional Laplacian operator, and applied the proposed algorithm to solve the fractional porous media equation. The proposed algorithm showed promising results on the benchmark problems where monotonous convergence was obtained and a consistent convergence rate was observed throughout multiple test cases. In the porous media equation case, the numerical solution coincided with the exact solution when the latter was available.

We conclude that isogeometric analysis is a viable tool for nonlocal problems modeled by the fractional Laplacian. For domains admitting a Cartesian grid discretization, meaning that the domain can be tessellated with squares (cubes), the finite difference method is applicable and easy to implement. The main challenge for many applications is that the domains are complex. The finite element method [17] is a standard approach to tackle complex domain and it works with the weak formulation of the partial differential equations. However, the implementation is substantially nontrivial for the fractional Laplacian due to the singularity in the integrand. Working with the strong form is easier but requires higher smoothness assumptions on the solution representation. The NURBS-based basis

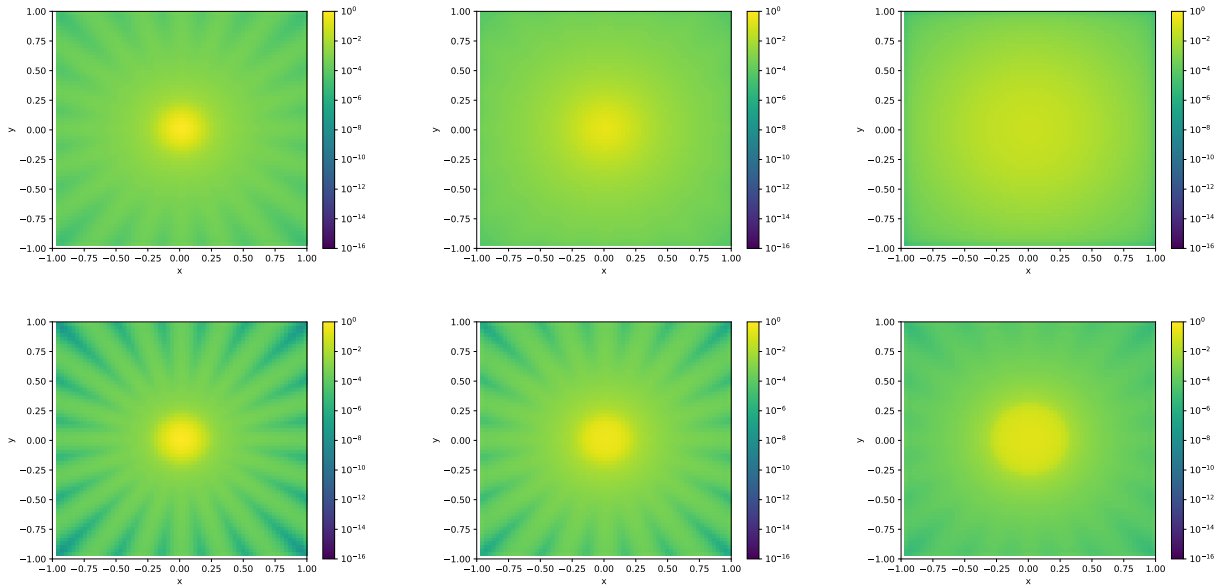


Figure 7: Solution to the porous media equation at $t = 0.1$. First row: $m = 1$, second row: $m = 2$; first column: $s = 0.2$, second column: $s = 0.5$, third column: $s = 0.8$. Note the logarithmic scale for colors.

functions in the isogeometric analysis are sufficiently smooth with appropriate degrees, thus we can work with the strong form directly and have simpler implementations. Moreover, the isogeometric analysis enables defining precisely many complex geometries (in this work, we worked with both the disk domain and the square domain) [19] and has higher accuracy per degree of freedom than the finite element analysis.

Despite the many strengths of our isogeometric collocation method, it requires precomputing \mathbf{L} in Algorithm 1, which can be very expensive since each quadrature point corresponding to the collocation point must be located. That is, we need to find the coordinates in the parameter space from the coordinates of the quadrature points in the physical space, which may require solving many nonlinear equations. This is not a problem with finite difference methods (when applicable) or finite element methods since those methods do not parametrize the physical domain.

In contrast to integer-order differential operators, fractional operators lead to denser coefficient matrices, which have higher storage and computational cost. However, the fractional Laplacian is an important tool when designing high fidelity models. An important next step is to develop efficient algorithms and explore the potential of isogeometric analysis for fractional PDEs; for examples, the computation of integrals based on quadrature rules can be accelerated using fast multiple method [7, 8, 34, 33, 38, 10, 9, 11, 14].

6. Acknowledgements

Kailai Xu thanks the Stanford Graduate Fellowship in Science & Engineering and the 2018 Schlumberger Innovation Fellowship for their financial support. Kailai Xu and Eric

Darve are also supported in part by the Applied Mathematics Program within the Department of Energy (DOE) Office of Advanced Scientific Computing Research (ASCR), through the Collaboratory on Mathematics and Physics-Informed Learning Machines for Multiscale and Multiphysics Problems Research Center (DESC0019453).

The appendix includes the basic concepts of isogeometric analysis which are relevant for our implementation.

Appendix A. Preliminary: Isogeometric Analysis

Appendix A.1. B-spline

We can describe B-splines in terms of a *knot vector* in the *parameter space*. A knot vector is specified by a non-decreasing set of coordinates

$$\mathcal{U} = \{u_1, u_2, \dots, u_{l+1}\} \quad (\text{A.1})$$

where u_i is called the *knot*, and satisfies

$$0 = u_1 = u_1 = \dots = u_{p+1} \leq u_{p+2} \leq \dots \leq u_{l-p} \leq u_{l-p+1} = u_{l-p+2} = \dots = u_{l+1} = 1 \quad (\text{A.2})$$

We allow the same value to occur multiple times and it will affect the continuity of the B-spline.

The i -th B-spline basis function of p -degree $N_{i,p}$ can be defined recursively as

$$B_{i,0}(u) = \begin{cases} 1 & \text{if } u_i \leq u < u_{i+1}, \\ 0 & \text{otherwise;} \end{cases} \quad (\text{A.3})$$

$$B_{i,p}(u) = \frac{u - u_i}{u_{i+p} - u_i} B_{i,p-1}(u) + \frac{u_{i+p+1} - u}{u_{i+p+1} - u_{i+1}} B_{i+1,p-1}(u) \quad (\text{A.4})$$

We note that B-splines have the following properties:

- The basis $B_{i,p}$ has compact support in $[u_i, u_{i+p+1}]$.
- For a knot vector of size $l + 1$, there are $l - p$ B-spline basis functions in total.
- They form a partition of unity, i.e.,

$$\sum_{i=1}^{l-p} B_{i,p} = 1 \quad (\text{A.5})$$

- Assume that all the inequalities in Eq. (A.2) are strict, then $B_{i,p} \in \mathcal{C}^{p-1}$ but $B_{i,p} \notin \mathcal{C}^p$.

Appendix A.2. NURBS

The NURBS basis function is created from B-splines by

$$N_{i,p}(u) = \frac{w_i B_{i,p}(u)}{\sum_{j=1}^{l-p} w_j B_{j,p}(u)} \quad (\text{A.6})$$

where w_i are $l - p$ weights assigned to each B-spline basis function. Bivariate NURBS are constituted by (suppressing the degrees p and q for u and v)

$$N_{k,l}(u, v) = \frac{w_{kl}B_k(u)B_l(v)}{\sum_{i=1}^{l_u-p} \sum_{j=1}^{l_v-q} w_{ij}B_i(u)B_j(v)} \quad (\text{A.7})$$

where $l_u + 1$ and $l_v + 1$ are the number of knots for u and v knot vectors.

A domain in one-dimension and two-dimension Cartesian space can be constructed with

$$\begin{aligned} X &= F(u) = \sum_{i=1}^{l-p} N_{i,p}(u) \tilde{X}_i \\ \mathbf{X} &= \mathbf{F}(u, v) = \sum_{i=1}^{l_u-p} \sum_{j=1}^{l_v-q} N_{k,l}(u, v) \tilde{\mathbf{X}}_{ij} \end{aligned} \quad (\text{A.8})$$

where \tilde{X}_i and $\tilde{\mathbf{X}}_{ij}$ are called *control points*. The equation Eq. (A.8) defines a mapping from parameter space to the physical space. Figure A.8 shows two examples of 2D domains constructed from NURBS basis functions. The red dots are the control points while the blue patches are subdomains corresponding to $[u_i, u_{i+1}] \times [v_j, v_{j+1}]$ in the parameter space.

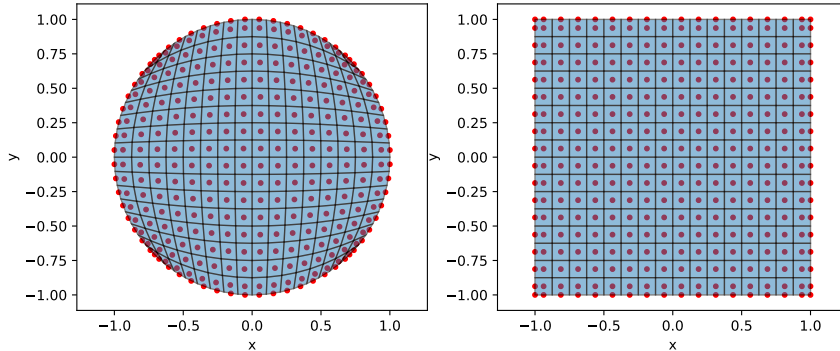


Figure A.8: Two examples of 2D domains constructed from NURBS basis functions. The red dots are the control points while the blue patches are subdomains corresponding to $[u_i, u_{i+1}] \times [v_j, v_{j+1}]$ in the parameter space.

In isogeometric analysis we use the same functions N_{kl} as basis functions for approximating the solutions. The interpolation function space is defined by a “push forward” operator

$$\mathbf{V} = \text{span}\{N_{kl} \circ \mathbf{F}^{-1}\}_{k=1,2,\dots,l_u-p; l=1,2,\dots,l_v-q} \quad (\text{A.9})$$

i.e., the numerical solution is given by

$$u_h(x, y) = \sum_{i=1}^{l_u-p} \sum_{j=1}^{l_v-q} N_{ij}(\mathbf{F}^{-1}(x, y)) c_{ij} \quad (\text{A.10})$$

where c_{ij} are coefficients determined by solving the governing equations.

Appendix A.3. Knot Insertion

The process of mesh refinement is critical to validate the numerical model. In isogeometric analysis, *knot insertion* provides us a way to easily refine the NURBS mesh. For any NURBS curve in the first formula of Eq. (A.8), we can view it as the projection of a B-spline curve in the two-dimensional space, where the coordinates are given as

$$\bar{\mathbf{X}}_i = [w_i \tilde{X}_i, w_i] \quad (\text{A.11})$$

Given the $l - p$ basis functions and the knot vector $\{u_1, u_2, \dots, u_{l+1}\}$, and $\bar{u} \in [u_k, u_{k+1})$ be a desired new knot, the new $l + 2$ control points $\{\bar{\mathbf{X}}_1^\dagger, \bar{\mathbf{X}}_2^\dagger, \dots, \bar{\mathbf{X}}_{l+2}^\dagger\}$ are formed from the original control points by

$$\bar{\mathbf{X}}_i^\dagger = \alpha_i \bar{\mathbf{X}}_i + (1 - \alpha_i) \bar{\mathbf{X}}_{i-1} \quad (\text{A.12})$$

where

$$\alpha_i = \begin{cases} 1 & 1 \leq i \leq k - p, \\ \frac{\bar{u} - u_i}{u_{i+p} - u_i} & k - p + 1 \leq i \leq k \\ 0 & k + 1 \leq i \leq l + 2 \end{cases} \quad (\text{A.13})$$

The new projected coordinates of the control points in the physical space are obtained using

$$\bar{X}_i^\dagger = \frac{(\bar{\mathbf{X}}_i^\dagger)_1}{(\bar{\mathbf{X}}_i^\dagger)_2} \quad (\text{A.14})$$

where $(\dots)_j$ denotes the j -th component. Knot insertion for two or higher dimension NURBS domains can be done separately for each dimension.

Appendix A.4. Computing the Coordinates in the Parameter Space

In the course of computing the fractional Laplacian, we need to compute the coordinate in the parametric space given its physical space location. NURBS does not provide a direct way to do this and thus a nonlinear equation is usually required to be solved. Specifically, given $\mathbf{x} = \begin{bmatrix} x \\ y \end{bmatrix}$, we want to find (u, v) such that

$$\mathbf{F}(u, v) = \sum_{i=1}^{l_u-p} \sum_{j=1}^{l_v-q} N_{i,j}(u, v) \tilde{\mathbf{X}}_{ij} = \begin{bmatrix} x \\ y \end{bmatrix} \quad (\text{A.15})$$

We can adopt the Gauss-Newton method for solving Eq. (A.15), where the gradient

$$\nabla \mathbf{F}(u, v) = \begin{bmatrix} \frac{\partial F_1}{\partial u} & \frac{\partial F_1}{\partial v} \\ \frac{\partial F_2}{\partial u} & \frac{\partial F_2}{\partial v} \end{bmatrix} \quad (\text{A.16})$$

is required. The gradient can be computed by noticing that

$$\begin{aligned}
S(u, v) &= \left(\sum_{i,j} w_{ij} B_i(u) B_j(v) \right)^2 \\
\frac{\partial N_{kl}(u, v)}{\partial u} &= \frac{w_{kl} B'_k(u) B_l(u) \sum_{i,j} w_{ij} B_i(u) B_j(v) - w_{kl} B_k(u) B_l(v) \sum_{i,j} w_{ij} B'_i(u) B_j(v)}{S(u, v)} \\
\frac{\partial N_{kl}(u, v)}{\partial v} &= \frac{w_{kl} B_k(u) B'_l(v) \sum_{i,j} w_{ij} B_i(u) B_j(v) - w_{kl} B_k(u) B_l(v) \sum_{i,j} w_{ij} B_i(u) B'_j(v)}{S(u, v)}
\end{aligned} \tag{A.17}$$

The algorithm for computing the coordinates in the parameter space is shown in Algorithm 2.

Algorithm 2 Gauss-Newton Method for Computing the Coordinates in the Parameter Space.

- 1: **Input:** \mathbf{x}_0 **Output:** \mathbf{u}
 - 2: Initialize $\mathbf{u} \leftarrow \begin{bmatrix} 0.5 \\ 0.5 \end{bmatrix}$, $\mathbf{x} \leftarrow \mathbf{F}(\mathbf{u})$
 - 3: **while** $|\mathbf{x}_0 - \mathbf{x}| > \text{tolerance}$ **do**
 - 4: $\mathbf{d} \leftarrow (\nabla \mathbf{F}(\mathbf{u}))^{-1} (\mathbf{x} - \mathbf{x}_0)$
 - 5: $\mathbf{u} \leftarrow \mathbf{u} - \mathbf{d}$
 - 6: $\mathbf{x} \leftarrow \mathbf{F}(\mathbf{u})$
 - 7: **end while**
 - 8: **return** \mathbf{u}
-

References

- [1] _____. https://www.uni-muenster.de/AMM/num/Vorlesungen/PDEI_SS14/material/slides.pdf. Lecture Notes.
- [2] Gabriel Acosta, Francisco M Bersetche, and Juan Pablo Borthagaray. A short FE implementation for a 2d homogeneous dirichlet problem of a fractional Laplacian. *Computers & Mathematics with Applications*, 74(4):784–816, 2017.
- [3] Mark Ainsworth and Christian Glusa. Aspects of an adaptive finite element method for the fractional Laplacian: a priori and a posteriori error estimates, efficient implementation and multigrid solver. *Computer Methods in Applied Mechanics and Engineering*, 327:4–35, 2017.
- [4] Mark Ainsworth and Christian Glusa. Towards an efficient finite element method for the integral fractional Laplacian on polygonal domains. *arXiv preprint arXiv:1708.01923*, 2017.
- [5] F Auricchio, L Beirao Da Veiga, TJR Hughes, A_ Reali, and G Sangalli. Isogeometric collocation methods. *Mathematical Models and Methods in Applied Sciences*, 20(11):2075–2107, 2010.
- [6] Yuri Bazilevs, L Beirao da Veiga, J Austin Cottrell, Thomas JR Hughes, and Giancarlo Sangalli. Isogeometric analysis: approximation, stability and error estimates for h-refined meshes. *Mathematical Models and Methods in Applied Sciences*, 16(07):1031–1090, 2006.
- [7] J Carrier, Leslie Greengard, and Vladimir Rokhlin. A fast adaptive multipole algorithm for particle simulations. *SIAM journal on scientific and statistical computing*, 9(4):669–686, 1988.
- [8] Hongwei Cheng, Leslie Greengard, and Vladimir Rokhlin. A fast adaptive multipole algorithm in three dimensions. *Journal of computational physics*, 155(2):468–498, 1999.
- [9] Pieter Coulier, Hadi Pouransari, and Eric Darve. The inverse fast multipole method: using a fast approximate direct solver as a preconditioner for dense linear systems. *SIAM Journal on Scientific Computing*, 39(3):A761–A796, 2017.
- [10] Eric Darve. The fast multipole method: numerical implementation. *Journal of Computational Physics*, 160(1):195–240, 2000.
- [11] Eric Darve, Cris Cecka, and Toru Takahashi. The fast multipole method on parallel clusters, multicore processors, and graphics processing units. *Comptes Rendus Mecanique*, 339(2-3):185–193, 2011.
- [12] Arturo de Pablo, Fernando Quirós, Ana Rodríguez, and Juan Luis Vázquez. A fractional porous medium equation. *arXiv preprint arXiv:1001.2383*, 2010.
- [13] Bartłomiej Dyda, Alexey Kuznetsov, and Mateusz Kwaśnicki. Eigenvalues of the fractional laplace operator in the unit ball. *Journal of the London Mathematical Society*, 95(2):500–518, 2017.
- [14] William Fong and Eric Darve. The black-box fast multipole method. *Journal of Computational Physics*, 228(23):8712–8725, 2009.
- [15] Paolo Gatto and Jan S Hesthaven. Numerical approximation of the fractional Laplacian via hp -finite elements, with an application to image denoising. *Journal of Scientific Computing*, 65(1):249–270, 2015.
- [16] Frédéric Gibou and Ronald Fedkiw. A fourth order accurate discretization for the laplace and heat equations on arbitrary domains, with applications to the stefan problem. *Journal of Computational Physics*, 202(2):577–601, 2005.
- [17] David Großmann, Bert Jüttler, Helena Schlusnus, Johannes Barner, and Anh-Vu Vuong. Isogeometric simulation of turbine blades for aircraft engines. *Computer Aided Geometric Design*, 29(7):519–531, 2012.
- [18] Mamikon Gulian, Maziar Raissi, Paris Perdikaris, and George Karniadakis. Machine learning of space-fractional differential equations. *SIAM Journal on Scientific Computing*, 41(4):A2485–A2509, 2019.
- [19] Behrooz Hassani, S Mehdi Tavakkoli, and NZ Moghadam. Application of isogeometric analysis in structural shape optimization. *Scientia Iranica*, 18(4):846–852, 2011.
- [20] MH Heydari, MR Hooshmandasl, FM Maalek Ghaini, and F Fereidouni. Two-dimensional Legendre wavelets for solving fractional poisson equation with dirichlet boundary conditions. *Engineering Analysis with Boundary Elements*, 37(11):1331–1338, 2013.
- [21] Mohammad Hossein Heydari and Zakieh Avazzadeh. Legendre wavelets optimization method for variable-order fractional poisson equation. *Chaos, Solitons & Fractals*, 112:180–190, 2018.
- [22] Mohammad Hossein Heydari, Zakieh Avazzadeh, and Malih Farzi Haromi. A wavelet approach for

- solving multi-term variable-order time fractional diffusion-wave equation. *Applied Mathematics and Computation*, 341:215–228, 2019.
- [23] Mohammad Hossein Heydari, Zakieh Avazzadeh, and Yin Yang. A computational method for solving variable-order fractional nonlinear diffusion-wave equation. *Applied Mathematics and Computation*, 352:235–248, 2019.
- [24] MR Hooshmandasl, MH Heydari, and C Cattani. Numerical solution of fractional sub-diffusion and time-fractional diffusion-wave equations via fractional-order Legendre functions. *The European Physical Journal Plus*, 131(8):268, 2016.
- [25] Yanghong Huang and Adam Oberman. Numerical methods for the fractional Laplacian: A finite difference-quadrature approach. *SIAM Journal on Numerical Analysis*, 52(6):3056–3084, 2014.
- [26] Thomas JR Hughes, John A Cottrell, and Yuri Bazilevs. Isogeometric analysis: CAD, finite elements, NURBS, exact geometry and mesh refinement. *Computer methods in applied mechanics and engineering*, 194(39-41):4135–4195, 2005.
- [27] Richard W Johnson. Higher order b-spline collocation at the greville abscissae. *Applied Numerical Mathematics*, 52(1):63–75, 2005.
- [28] Mateusz Kwaśnicki. Ten equivalent definitions of the fractional laplace operator. *Fractional Calculus and Applied Analysis*, 20(1):7–51, 2017.
- [29] Andreas E Kyprianou, Ana Osójnik, and Tony Shardlow. Unbiased ‘walk-on-spheres’ monte carlo methods for the fractional Laplacian. *IMA Journal of Numerical Analysis*, 38(3):1550–1578, 2017.
- [30] Anna Lischke, Guofei Pang, Mamikon Gulian, Fangying Song, Christian Glusa, Xiaoning Zheng, Zhiping Mao, Wei Cai, Mark M Meerschaert, Mark Ainsworth, et al. What is the fractional Laplacian? *arXiv preprint arXiv:1801.09767*, 2018.
- [31] Boris Maryshev, Alain Cartalade, Christelle Latrille, Maminirina Joelson, and Marie-Christine Néel. Adjoint state method for fractional diffusion: parameter identification. *Computers & Mathematics with Applications*, 66(5):630–638, 2013.
- [32] V. Minden and L. Ying. A simple solver for the fractional Laplacian in multiple dimensions. *ArXiv e-prints*, February 2018.
- [33] Naoshi Nishimura. Fast multipole accelerated boundary integral equation methods. *Applied mechanics reviews*, 55(4):299–324, 2002.
- [34] Naoshi Nishimura, Ken-ichi Yoshida, and Shoichi Kobayashi. A fast multipole boundary integral equation method for crack problems in 3d. *Engineering Analysis with Boundary Elements*, 23(1):97–105, 1999.
- [35] Łukasz Płociniczak. Approximation of the Erdélyi–Kober operator with application to the time-fractional porous medium equation. *SIAM Journal on Applied Mathematics*, 74(4):1219–1237, 2014.
- [36] Alessandro Reali and Thomas JR Hughes. An introduction to isogeometric collocation methods. In *Isogeometric Methods for Numerical Simulation*, pages 173–204. Springer, 2015.
- [37] Xavier Ros-Oton and Joaquim Serra. The dirichlet problem for the fractional Laplacian: regularity up to the boundary. *Journal de Mathématiques Pures et Appliquées*, 101(3):275–302, 2014.
- [38] JM Song and Weng Cho Chew. Multilevel fast-multipole algorithm for solving combined field integral equations of electromagnetic scattering. *Microwave and Optical Technology Letters*, 10(1):14–19, 1995.
- [39] I Temizer, P Wriggers, and TJR Hughes. Contact treatment in isogeometric analysis with nurbs. *Computer Methods in Applied Mechanics and Engineering*, 200(9-12):1100–1112, 2011.
- [40] Yufeng Wang, Hui Zhou, Hanming Chen, and Yangkang Chen. Adaptive stabilization for Q-compensated reverse time migration. *Geophysics*, 83(1):S15–S32, 2017.
- [41] Kailai Xu and Eric Darve. Calibrating multivariate Lévy processes with neural networks. *arXiv preprint arXiv:1812.08883*, 2018.
- [42] Kailai Xu and Eric Darve. Spectral method for the fractional Laplacian in 2d and 3d. *arXiv preprint arXiv:1812.08325*, 2018.
- [43] Yiran Xu, Jingye Li, Guofei Pang, Zhikai Wang, and Xiaohong Chen. Radial basis function collocation method for decoupled fractional Laplacian wave equations. *arXiv preprint arXiv:1801.01206*, 2018.